PHYSICAL REVIEW D **88,** 056007 (2013)

Quark spectral function and deconfinement at nonzero temperature

Si-xue Qin[1,*] and Dirk H. Rischke[1,2,†]

[1]*Institute for Theoretical Physics, Johann Wolfgang Goethe University, Max-von-Laue-Strasse 1, D-60438 Frankfurt am Main, Germany*

[2]*Frankfurt Institute for Advanced Studies, Ruth-Moufang-Strasse 1, D-60438 Frankfurt am Main, Germany*

(Received 26 April 2013; published 5 September 2013)

The maximum entropy method is used to compute the quark spectral function at nonzero temperature. We solve the gap equation of quantum chromodynamics (QCD) self-consistently, employing a rainbow kernel which phenomenologically models results from Dyson-Schwinger equations and lattice QCD. We use the criterion of positivity restoration of the spectral function as a signal for deconfinement. Our calculation indicates that the critical temperature of deconfinement T_d is slightly smaller than the one of chiral symmetry restoration T_c: $T_d \sim 94\% T_c$ in the chiral limit and $T_d \sim 96\% T_c$ with physical light quark masses. Since these deviations are within the systematic error of our approach, it is reasonable to conclude that chiral symmetry restoration and deconfinement coincide at zero chemical potential.

DOI: 10.1103/PhysRevD.88.056007 PACS numbers: 11.10.Wx, 11.15.Tk, 12.38.Mh, 24.85.+p

I. INTRODUCTION

Heavy-ion experiments at the Relativistic Heavy-Ion Collider and the Large Hadron Collider are focusing on charting the phase diagram of hot and dense nuclear matter. The quark-gluon plasma (QGP), a primordial state of matter in the early Universe, where chiral symmetry is restored and quarks and gluons are deconfined, has been recreated in the extremely hot environment of a heavy-ion collision. With the expansion of the fireball, nuclear matter cools down and dilutes. The low-temperature, low-density phase of nuclear matter is characterized by confinement and dynamical chiral symmetry breaking (DCSB). It is a central goal of modern theoretical physics to understand the properties of, and the transitions between, these phases. The chiral and deconfinement phase transitions as well as their interplay are especially interesting. In general, the chiral condensate (or, equivalently, the dynamical quark mass) is adopted as an order parameter for the chiral phase transition. The order of this transition may depend on the number of quark flavors, the values of the quark masses, and whether the $U(1)_A$ anomaly of QCD is effectively restored. For nonzero quark masses, the existence of a critical end point (where the transition turns from being first order at low temperatures and high densities to being crossover at high temperatures and low densities) has been suggested but, even if it exists at all, its precise location is still highly debated.

Concerning the deconfinement phase transition, the situation is even more complicated because confinement has been a mystery since the inception of the Standard Model. The notion of confinement is easily understood from the linearly rising potential between infinitely heavy quarks [1,2], which has also been studied by lattice QCD [3]. However, this is no longer true for light quarks because of strong pair-creation and pair-annihilation effects [4]. In the pure-gauge limit realized for infinitely heavy quarks, the center $Z(3)$ symmetry of the color gauge group $SU(3)$ is preserved in the confining phase, while it is spontaneously broken in the deconfined phase. Here, the Polyakov loop (or the thermal Wilson line) [5,6] is the corresponding order parameter. Equivalently, the dual quark condensate [7–9] was proposed as an order parameter, which makes it possible to study the interplay between confinement and DCSB. However, their validity as order parameters for phase transitions in light quark systems remains unclear.

Besides these order parameters, confinement can be related to the analytic properties of QCD Schwinger functions [10–12]. The axiom of reflection positivity requires that the propagator has a positive definite Källen-Lehmann spectral representation for asymptotic (or deconfined) quarks. In other words, if the quark propagator can be decomposed in terms of complete eigenstates of the Hamiltonian, each of which should have positive probability, quarks can propagate as asymptotic states; otherwise, quarks have to be somehow confined. It can be shown that pairs of complex conjugate poles of the full quark propagator lead to a nonpositive definite Källen-Lehmann spectral representation. Therefore, in Refs. [13,14], the existence of such pairs of complex conjugate poles was considered as a criterion for confinement. However, this is only a sufficient condition. The reason is that the violation of reflection positivity can also be realized by propagators with real poles, namely, if they have a negative residue which also leads to the Källen-Lehmann spectral representation being not positive definite [15]. On the other hand, the positivity of the quark spectral function is a necessary and sufficient condition for quark deconfinement, no matter whether the singularities of the quark propagator are located on or off the real axis. In short, by considering the quark spectral function directly, one is able to distinguish confined phases (where

*sixueqin@th.physik.uni-frankfurt.de
†drischke@th.physik.uni-frankfurt.de

reflection positivity is violated) from deconfined ones (where reflection positivity holds).

In this work, we use the maximum entropy method (MEM) [16–19] to explicitly compute quark spectral functions from the self-consistent numerical solution of the QCD gap equation. We employ a rainbow kernel [20,21] which phenomenologically models recent results from Dyson-Schwinger equations (DSE) [22,23] and lattice QCD [24–26]. We define a deconfinement temperature as the temperature above which the positivity of the quark spectral function is restored. This work is a continuation of Ref. [27] where the quark spectral functions were studied in the region above T_c. This paper is organized as follows. In Sec. II, we present the QCD gap equation and discuss the ansatz employed for its solution. In Sec. III, we derive the relation between the quark spectral function and the solution of the gap equation. Here, we also define the order parameter which signals the positivity of the spectral function. In Sec. IV, we briefly outline the MEM and its extension for nonpositive definitive spectral functions. Section V reports our numerical results. Finally, we conclude with a summary and some remarks.

II. QCD GAP EQUATION

At nonzero temperature, the QCD gap equation is

$$S(i\omega_n, \vec{p})^{-1} = i\vec{\gamma}\cdot\vec{p} + i\gamma_4\omega_n + m + \Sigma(i\omega_n, \vec{p}), \quad (1)$$

$$\Sigma(i\omega_n, \vec{p}) = \frac{4T}{3}\sum_{l=-\infty}^{+\infty}\int\frac{d^3\vec{q}}{(2\pi)^3}\, g^2 D_{\mu\nu}(\vec{k}, \Omega_{nl}) \times \gamma_\mu S(i\omega_l, \vec{q})\Gamma_\nu(\vec{q}, \omega_l, \vec{p}, \omega_n), \quad (2)$$

where $\omega_n = (2n+1)\pi T$ is the fermionic Matsubara frequency, $\vec{k} = \vec{p} - \vec{q}$, $\Omega_{nl} = \omega_n - \omega_l$, $D_{\mu\nu}$ is the dressed gluon propagator, and Γ_ν is the dressed quark-gluon vertex. The solution of the gap equation can be expressed as

$$S(i\omega_n, \vec{p})^{-1} = i\vec{\gamma}\cdot\vec{p}A(\omega_n^2, \vec{p}^2) + i\gamma_4\omega_n C(\omega_n^2, \vec{p}^2) + B(\omega_n^2, \vec{p}^2) \quad (3)$$

or, equivalently,

$$S(i\omega_n, \vec{p}) = -i\vec{\gamma}\cdot\vec{p}\sigma_A(\omega_n^2, \vec{p}^2) - i\gamma_4\omega_n\sigma_C(\omega_n^2, \vec{p}^2) + \sigma_B(\omega_n^2, \vec{p}^2), \quad (4)$$

where A, B, C, and $\sigma_{A,B,C}$ are scalar functions. The dynamical quark mass is defined as $M(\omega_n^2, \vec{p}^2) = B(\omega_n^2, \vec{p}^2)/A(\omega_n^2, \vec{p}^2)$, which is independent of the renormalization point. In the chiral limit, the chiral condensate is defined as

$$-\langle\bar{q}q\rangle^0 = N_c T\sum_{n=-\infty}^{+\infty}\int\frac{d^3\vec{p}}{(2\pi)^3}\,\mathrm{tr}_D S(i\omega_n, \vec{p}), \sim M(\omega_0^2, \vec{p}^2 = 0). \quad (5)$$

However, because of an ultraviolet divergence the integral in the above equation is not well defined at nonzero current quark mass. Conveniently, $M_0 := M(\omega_0^2, \vec{p}^2 = 0)$ can be used as the order parameter for the chiral phase transition, which is equivalent to the chiral condensate.

The gap equation is closed by specifying the vertex and the gluon propagator. Here, we use the rainbow truncation, i.e., the leading term in a symmetry-preserving scheme [28]:

$$g^2 D_{\mu\nu}(\vec{k}, \Omega_{nl})\Gamma_\nu(\vec{q}, \omega_l, \vec{p}, \omega_n) = [P^T_{\mu\nu}D_T(\vec{k}^2, \Omega_{nl}^2) + P^L_{\mu\nu}D_L(\vec{k}^2, \Omega_{nl}^2)]\gamma_\nu, \quad (6)$$

where $P^{T,L}_{\mu\nu}$ are transverse and longitudinal projection operators, respectively,

$$P^T_{\mu\nu} = \begin{cases} 0 & \mu \quad \text{and/or} \quad \nu = 4, \\ \delta_{ij} - \frac{\vec{k}_i\vec{k}_j}{\vec{k}^2}, & \mu, \nu = 1, 2, 3, \end{cases} \quad (7)$$

$$P^L_{\mu\nu} = \delta_{\mu\nu} - \frac{k^\mu_\Omega k^\nu_\Omega}{k^2_\Omega} - P^T_{\mu\nu}, \quad (8)$$

with $k_\Omega := (\Omega_{nl}, \vec{k})$, and where

$$D_T = \mathcal{D}(\vec{k}^2 + \Omega_{nl}^2), \qquad D_L = \mathcal{D}(\vec{k}^2 + \Omega_{nl}^2 + m_g^2). \quad (9)$$

Here, the function

$$\mathcal{D}(s) = \frac{8\pi^2 D}{\sigma^4}e^{-s/\sigma^2} + \frac{8\pi^2\gamma_m}{\ln[\tau + (1 + s/\Lambda^2_{\mathrm{QCD}})^2]}\mathcal{F}(s), \quad (10)$$

with $\mathcal{F}(s) = [1 - \exp(-s/4m_t^2)]/s$, $\tau = e^2 - 1$, $m_t = 0.5$ GeV, $\gamma_m = 12/25$, and $\Lambda^{N_f=4}_{\mathrm{QCD}} = 0.234$ GeV. For pseudoscalar and vector mesons with masses $\lesssim 1$ GeV, this interaction provides a uniformly good description of their vacuum properties when $\sigma D = (0.8\ \mathrm{GeV})^3$ and $\sigma \in [0.4, 0.6]$ GeV [20,21], which means that there is only one free parameter in the model. The physical masses of the light quarks are $m^\zeta_{u=d} = 3.4$ MeV at our renormalization point $\zeta = 19$ GeV. Generalizing to $T \neq 0$, we have followed perturbation theory and included a Debye-like mass in the longitudinal part of the gluon propagator: $m_g^2 = (16/5)T^2$ (for details, see Ref. [27]).

III. SPECTRAL REPRESENTATION

The dressed quark propagator is related to the retarded real-time propagator by analytic continuation,

$$S^R(\omega, \vec{p}) = S(i\omega_n, \vec{p})|_{i\omega_n\to\omega+i\epsilon}. \quad (11)$$

From the spectral representation of $S^R(\omega, \vec{p})$, i.e.,

$$\rho(\omega, \vec{p}) = -2\Im S^R(\omega, \vec{p}), \quad (12)$$

one immediately obtains

$$S(i\omega_n, \vec{p}) = \int_{-\infty}^{+\infty}\frac{d\omega'}{2\pi}\frac{\rho(\omega', \vec{p})}{i\omega_n - \omega'}. \quad (13)$$

According to Eq. (4), the spectral function can be decomposed as

$$\rho(\omega,\vec{p}) = -i\vec{\gamma}\cdot\vec{p}\,\rho_v(\omega,\vec{p}^2) + \gamma_4\omega\rho_e(\omega,\vec{p}^2) + \rho_s(\omega,\vec{p}^2). \tag{14}$$

As a consequence of the anticommutation relation, the spectral function fulfills the following sum rule:

$$\int_{-\infty}^{+\infty}\frac{d\omega}{2\pi}\rho(\omega,\vec{p})\gamma_4 = \mathbf{1}. \tag{15}$$

Then one can define the spectral function $\rho_0(\omega,\vec{p}^2) := \omega\rho_e(\omega,\vec{p}^2)$, which is non-negative and can be treated as a probability distribution for deconfined quarks. Note that $\rho_0(\omega,\vec{p}^2)$ can be easily related to the dressed quark propagator by

$$\begin{aligned} S_0(\omega_n^2,\vec{p}^2) &= i\omega_n\sigma_C(\omega_n^2,\vec{p}^2) \\ &= \int_{-\infty}^{+\infty}\frac{d\omega'}{2\pi}\frac{\rho_0(\omega',\vec{p}^2)}{\omega'-i\omega_n}, \end{aligned} \tag{16}$$

where σ_C is the scalar function in Eq. (4), or to the imaginary-time quark propagator

$$\begin{aligned} D_0(\tau,\vec{p}^2) &= T\sum_n e^{-i\omega_n\tau}S_0(\omega_n^2,\vec{p}^2), \\ &= \int_{-\infty}^{+\infty}\frac{d\omega}{2\pi}\frac{e^{(1/2-\tau T)\omega/T}}{e^{\omega/2T}+e^{-\omega/2T}}\rho_0(\omega,\vec{p}^2). \end{aligned} \tag{17}$$

The above equations connect the quark spectral function which we consider to the numerical solution of the gap equation. As a signal for positivity violation (or restoration) of the spectral function, one can define an "order" parameter as

$$\hat{Z}_\rho = \int_{-\infty}^{+\infty}\frac{d\omega}{2\pi}|\rho(\omega)|, \tag{18}$$

$$Z_\rho = \int_{-\infty}^{+\infty}\frac{d\omega}{2\pi}\rho(\omega), \tag{19}$$

$$L_\rho = \frac{\hat{Z}_\rho - Z_\rho}{\hat{Z}_\rho}, \tag{20}$$

where $\rho(\omega)$ simply denotes $\rho_0(\omega,\vec{p}^2=0)$. It is apparent that $\hat{Z}_\rho = Z_\rho = 1$ and $L_\rho = 0$ for a positive definite spectral function; otherwise $\hat{Z}_\rho > Z_\rho = 1$ and $L_\rho > 0$. The critical temperature T_d of the deconfinement transition is defined as the lowest temperature where $L_\rho = 0$.

IV. MAXIMUM ENTROPY METHOD

It is an ill-posed problem to extract the spectral function from the (imaginary-time) quark propagator. Actually, there is an infinite set of spectral functions which can reproduce a given correlation function with tolerable errors. The MEM [16–19] considers the probability distribution of spectral functions to produce the most probable one. The theoretical basis is Bayes's probability theorem. The conditional probability of having the spectral function $\rho(\omega)$ given the correlation function $D(\tau)$ reads

$$P[\rho|DM] = \frac{P[D|\rho M]P[\rho|M]}{P[D|M]}, \tag{21}$$

where M summarizes all definitions and prior knowledge of the spectral function, $P[D|\rho M]$ and $P[\rho|M]$ are called the likelihood function and the prior probability, respectively. Since $P[D|M]$ is independent of $\rho(\omega)$, it can be treated as a normalization constant.

According to the central-limit theorem the data $D(\tau)$ are expected to obey a Gaussian distribution:

$$P[D|\rho M] = \frac{1}{Z_L}e^{-L[\rho]}, \tag{22}$$

with

$$L[\rho] = \frac{1}{\beta}\int_0^\beta d\tau\frac{|D(\tau)-D[\rho](\tau)|^2}{2\xi(\tau)^2}, \tag{23}$$

where Z_L is a normalization constant, $D[\rho]$ denotes the correlation function reproduced by Eqs. (16) or (17) given the spectral function $\rho(\omega)$, and $\xi(\tau)$ is the variance of the error. Maximizing the likelihood function is equivalent to χ^2 fitting.

The construction of the prior probability $P[\rho|M]$ is the central idea of MEM, which expresses the prior in terms of the spectral entropy as

$$P[\rho|M(\alpha)] = \frac{1}{Z_S}e^{\alpha S[\rho,m]}, \tag{24}$$

where Z_S is a normalization constant and α is an undetermined positive scale factor. The Shannon-Jaynes entropy S is defined as

$$S[\rho,m] = \int_{-\infty}^{+\infty}d\omega\left[\rho(\omega)-m(\omega)-\rho(\omega)\ln\frac{\rho(\omega)}{m(\omega)}\right], \tag{25}$$

where $m(\omega)$ is the "default model" of the spectral function. Its typical form is a uniform distribution without *a priori* structure assumption [27], i.e.,

$$m(\omega) = m_0\theta(\Lambda^2-\omega^2). \tag{26}$$

Note that a reliable output from the MEM should be insensitive to the choice of m_0 and Λ. Let us therefore elaborate further on the choice of the default model. For the convergence of the integral in Eq. (15), the spectral function should decrease faster than ω^{-1} as $\omega\to\infty$. Our default model Eq. (26) is just one particular choice that fulfills this criterion because it simply sets the high-energy tail of $m(\omega)$ to zero. The MEM, however, simply copies this behavior into the spectral function which then also vanishes at high energy. One may then argue that the

high-energy behavior of the default model may cause some artificial behavior of the high-energy part of the spectral function. Nevertheless, since the integration kernel in Eq. (17) is exponentially damped, the high-energy behavior of the spectral function does not have a significant impact on the Euclidean correlator. Therefore, we also do not expect a significant influence of the choice of Λ (or, more generally, the precise form of the high-energy behavior of the default model) on our results.

On the other hand, for the same reason the Euclidean correlator is strongly affected by the low- and intermediate-energy behavior of the spectral function. Note that the positivity violation of the spectral function happens precisely in this region, i.e., for $|\omega| < \Lambda$. We therefore expect some sensitivity of the Euclidean correlator to our choice of m_0. This will be further investigated below.

If the spectral function is not positive definite, one can decompose it in terms of two positive definite components, i.e.,

$$\rho(\omega) = \rho_+(\omega) - \rho_-(\omega), \tag{27}$$

Correspondingly, the total entropy is expressed as [29,30]

$$S[\rho, m] = S[\rho_+, m_+] + S[\rho_-, m_-], \tag{28}$$

where $m_\pm$ denotes the default models of $\rho_\pm$, respectively. Note that we assume $S[\rho_+, m_+]$ and $S[\rho_-, m_-]$ to enter with equal weights in Eq. (28). In principle, one could choose unequal weights, but this would change the subsequent formulas. At first glance, Eqs. (27) and (28) suggest that there is an infinite number of choices for ρ_+ and ρ_- that lead to the same spectral function ρ. However, this is not the case which can be seen as follows. From the definition, i.e., Eqs. (27) and (28), we always have $\delta S/\delta\rho = \pm\delta S/\delta\rho_\pm$ and then

$$\frac{\delta S}{\delta\rho_+} + \frac{\delta S}{\delta\rho_-} = 0, \tag{29}$$

which leads to the constraint $\rho_+\rho_- = m_+m_-$ via Eq. (25). Then, we can rewrite $\rho_\pm$ as

$$\rho_\pm(\omega) = \frac{\hat\rho(\omega) \pm \rho(\omega)}{2}, \tag{30}$$

where $\hat\rho = [\rho^2 + 4m_+m_-]^{1/2}$. Inserting Eq. (30) into Eq. (28), we obtain

$$S[\rho, m] = \int_{-\infty}^{+\infty} d\omega \Bigg(\hat\rho(\omega) - m_+(\omega) - m_-(\omega) - \rho(\omega) \times \ln\left[\frac{\hat\rho(\omega) + \rho(\omega)}{2m_+(\omega)}\right] \Bigg), \tag{31}$$

which removes the explicit dependence of the entropy on $\rho_\pm$ by expressing it solely as a function of ρ and $m_\pm$. In Ref. [29] it was shown that such a form of the entropy can be obtained by direct counting arguments. Rewriting Eq. (25) in the form Eq. (31), one can extend MEM to a wider range of applications (e.g., see Ref. [31]). Compared with Eq. (25), there are two default models, $m_\pm$, in Eq. (31). Since the difference $m_+ - m_-$ is the default model of ρ, we can choose the default models as

$$\begin{aligned} m_+(\omega) &= \frac{(1+\eta)\pi}{\Lambda}\theta(\Lambda^2 - \omega^2), \\ m_-(\omega) &= \frac{\eta\pi}{\Lambda}\theta(\Lambda^2 - \omega^2), \end{aligned} \tag{32}$$

where the prior information on ρ, i.e., the sum rule Eq. (15), has been taken into account. The parameter η can be changed in a large range, e.g., $\eta \in [0.1, 10]$, in order to analyze the sensitivity of the output on the choice of η and to perform an error analysis.

Finally, one obtains the total probability distribution

$$P[\rho|DM(\alpha)] \propto e^{\alpha S[\rho,m] - L[\rho]}. \tag{33}$$

The most probable spectral function $\rho_\alpha(\omega)$ for fixed α can be obtained by maximizing $P[\rho|DM(\alpha)]$, where usually the standard singular-value decomposition algorithm of Bryan [16] is adopted. To deal with the scale factor α, we follow Bryan's method [16]. The MEM spectral function is defined as

$$\begin{aligned} \rho_{\mathrm{MEM}} &= \int_0^\infty d\alpha \int \mathcal{D}\rho\,\rho(\omega) P[\rho|DM(\alpha)] P[\alpha|DM] \\ &\simeq \int_0^\infty d\alpha\, \rho_\alpha(\omega) P[\alpha|DM], \end{aligned} \tag{34}$$

where it is assumed that $P[\rho|DM(\alpha)]$ is sharply peaked around $\rho_\alpha(\omega)$, so that the functional integral over ρ can be approximated. In this way, the MEM spectral function becomes an average of the $\rho_\alpha(\omega)$'s with respect to α. The conditional probability $P[\alpha|DM]$ can be evaluated using Bayes's theorem as

$$P[\alpha|DM] = \int \mathcal{D}\rho P[\rho|DM(\alpha)] P[\alpha|M] \tag{35}$$

$$\propto P[\alpha|M] \int \mathcal{D}\rho e^{\alpha S[\rho,m] - L[\rho]}. \tag{36}$$

Using the saddle-point approximation and the Laplace rule ($P[\alpha|M] = \text{const}$), one obtains

$$P[\alpha|DM] \propto \exp\left(\frac{1}{2}\sum_k \ln\frac{\alpha}{\alpha + \lambda_k} + \alpha S[\rho_\alpha, m] - L[\rho_\alpha] \right),$$

where the λ_k are eigenvalues of the following real symmetric matrix in functional space:

$$\Lambda_{ij} = \sqrt{\hat\rho_i}\frac{\partial^2 L}{\partial\rho_i\partial\rho_j}\sqrt{\hat\rho_j}\,\Big|_{\rho=\rho_\alpha}. \tag{37}$$

Normalizing $P[\alpha|DM]$ and using Eq. (34) one finally obtains ρ_{MEM}.

V. NUMERICAL RESULTS

At zero temperature, $T = 0$, the largest contribution to the constituent quark mass comes from DCSB which dominates low-energy hadron physics. With increasing temperature, $T > 0$, the dynamical quark mass decreases, which indicates a partial restoration of chiral symmetry. In the chiral limit, there exists a critical temperature T_c where the dynamical quark mass drops to zero and chiral symmetry is completely restored through a second-order phase transition [32]. Because of nonzero current quark masses, chiral symmetry is not exact. Instead of a second-order phase transition, a crossover happens at some pseudocritical temperature T_c which is defined by the steepest-descent point for the dynamical quark mass. For these two cases, the behavior of the dynamical quark masses with temperature is illustrated in the upper panel of Fig. 1. The (pseudo)critical temperatures have been indicated as vertical lines.

Using our model parameters which are able to provide a uniformly good description of vacuum properties of pseudoscalar and vector mesons with masses $\lesssim 1$ GeV, we calculate the dependence of the (pseudo)critical temperatures on the interaction width σ, which is shown in the lower panel of Fig. 1: T_c monotonically decreases with increasing σ. This behavior is consistent with results obtained in Ref. [32]. Remarkably, the critical temperature range overlaps well with that obtained by lattice QCD, i.e., $T_c \in [0.146, 0.170]$ GeV [33].

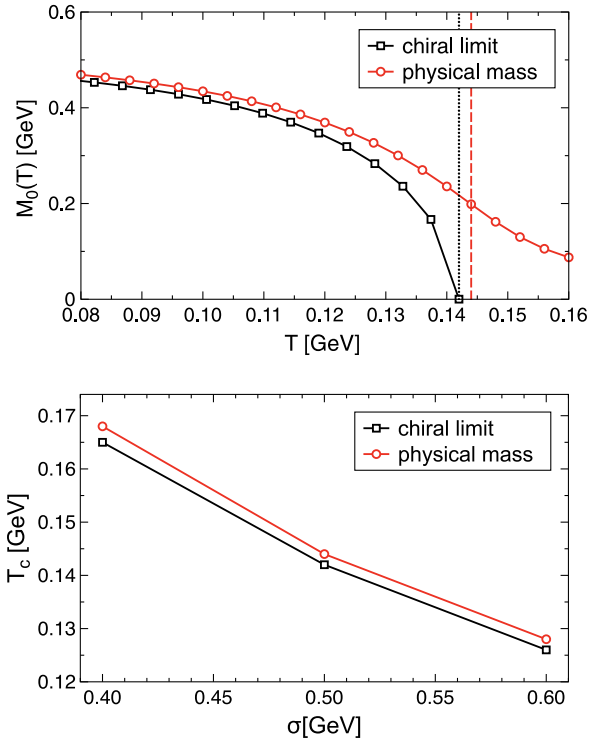

FIG. 1 (color online). Upper panel: Behavior of the dynamical quark mass with temperature (for $\sigma = 0.5$ GeV). The black line marked by squares is the chiral limit; the red line marked by circles is for the physical value of the current quark mass. The black dotted line denotes the critical temperature T_c of the second-order phase transition in the chiral limit; the red dashed line denotes the steepest-descent point for the dynamical quark mass, i.e., the pseudocritical temperature for the physical current quark mass. Lower panel: Dependence of the (pseudo)critical temperature T_c on the interaction width σ in our model.

Above the critical temperature T_c, the quark spectral function has been studied by both perturbative and nonperturbative approaches. At $T > 3T_c$ where perturbation theory (hard-thermal-loop resummation) works, the properties of the QGP are dominated by two collective excitations: thermal and plasmino excitations [34]. At $T \gtrsim T_c$, experimental observables indicate that nuclear matter is a strongly coupled QGP (sQGP) [35]. In this temperature region, perturbation theory fails while the nonperturbative DSE approach predicts a novel zero excitation mode in addition to the normal thermal and plasmino ones [27]. The typical behavior of the quark spectral function is illustrated in Fig. 2. Here, the spectral function is positive definite and each peak corresponds to an excitation mode.

Below the critical temperature T_c, the system is nonperturbative because of DCSB and/or confinement. Nevertheless, the spectral function computed from the solution of the truncated gap equation can provide some nontrivial information about the system.

References [10–12] have indicated that, in a log plot of the absolute magnitude, the Euclidean correlator is not convex at very low temperature or, equivalently, that the Euclidean correlator becomes negative in a range around $\tau T = 1/2$. Note that the kernel of the spectral representation, i.e., Eq. (17), is always a positive definite exponential function. This means that a positive definite spectral function can only produce a positive definite Euclidean correlator. Therefore, the spectral function must be negative in (at least) one range of energy, which also has to dominate the integral, in order for a nonpositive (nonconvex) correlator to emerge. With increasing temperature, the contribution of the negative component decreases. Therefore,

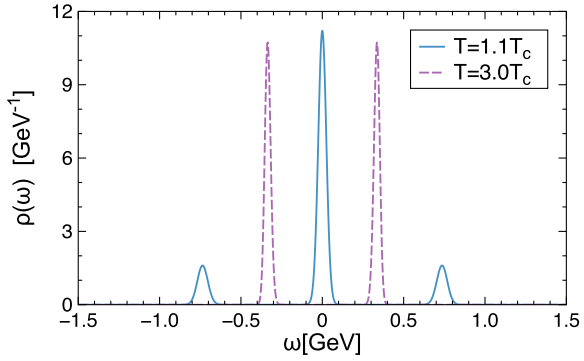

FIG. 2 (color online). Typical behavior of the spectral function at $T > T_c$ (following Ref. [27]).

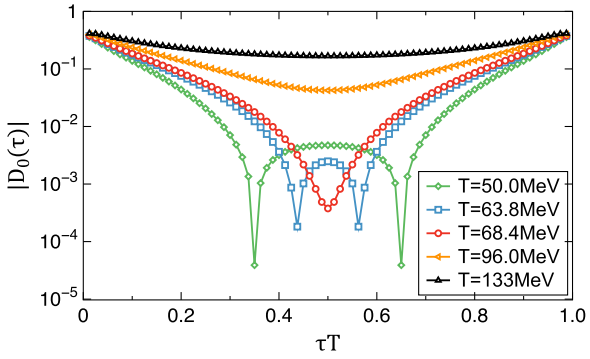

FIG. 3 (color online). The Euclidean correlator at different temperatures ($\sigma = 0.5$ GeV, chiral limit).

there exists a temperature where the Euclidean correlator becomes positive definite (convex in a log plot of its absolute value), although, as we will explicitly demonstrate below, the spectral function still has negative components. This is shown in Fig. 3: the (logarithm of the absolute magnitude of the) Euclidean correlator is not a convex function at low temperatures, but becomes convex at $T \sim 70$ MeV ($\sim 0.5T_c$), at which temperature, as we shall see below, the spectral function should still be not positive definite. Thus, the nonconvexity of the Euclidean correlator is only a sufficient, but not a necessary condition for the positivity violation of the spectral function. We therefore now focus on computing the spectral function explicitly.

To implement the MEM spectral analysis, we typically prepare 64 equal-interval data points with a relative standard deviation around 2×10^{-4} for the Euclidean correlators. We calculate the quark spectral function at $T = 0.8T_c$ with the interaction width $\sigma = 0.5$ GeV and in the chiral limit, which is plotted in Fig. 4. It is found that the quark spectral function exhibits some negative peaks and thus obviously $L_\rho > 0$. The shaded region around the curve in Fig. 4 corresponds to the variation of the parameter η in the default model (32) in the range [0.1, 10]. One observes that the shape of the spectral function is very robust in this range of η values. Also, the order parameter L_ρ only changes by about 1% under such variation.

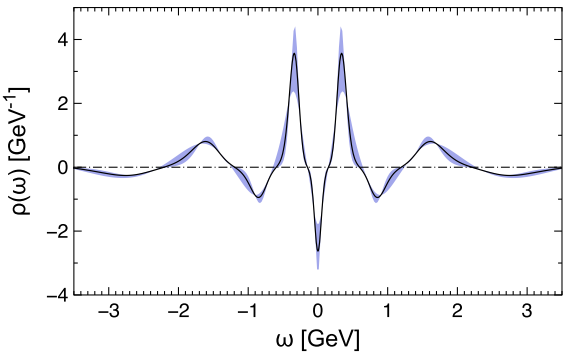

FIG. 4 (color online). The behavior of the quark spectral function at $T = 0.8T_c$ ($\sigma = 0.5$ GeV, chiral limit).

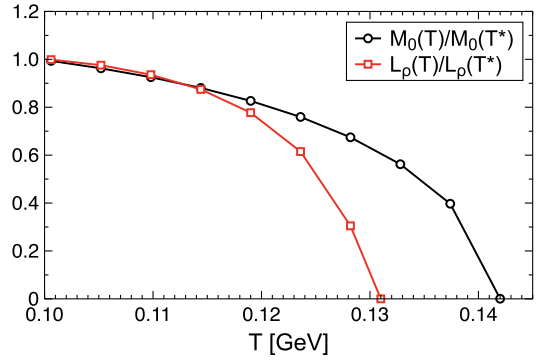

FIG. 5 (color online). The dynamical quark mass M_0 and the deconfinement order parameter L_ρ as a function of temperature ($T^* = 0.1$ GeV, $\sigma = 0.5$ GeV, chiral limit).

Moreover, the MEM error bar analysis indicates a quite small relative standard deviation σ_{MEM} for the resulting spectral function, e.g., σ_{MEM} is around $2\times10^{-4}\sim2\times10^{-2}$ for the peaks in the interval [0, 3] GeV. It is therefore very reasonable to conclude that the negative peaks of the spectral function are real structures and not an artifact of our analysis.

Although the physical meaning of those negative peaks is unclear, it still makes sense to analyze how their behavior changes with temperature. We found that the structure of the nonpositive spectral function remains unchanged while the residues of the negative peaks, i.e., L_ρ, decrease with increasing temperature. Notably, there exists a critical temperature T_d where L_ρ drops to zero, which signals the positivity restoration of the spectral function and deconfinement. The calculated behavior of L_ρ is shown in Fig. 5 in comparison with that of the dynamical mass M_0, which indicates that $T_d \lesssim T_c$. Next, we calculate the dependence of T_d on the interaction width σ both in the chiral limit and with a physical current quark mass, which is shown in Fig. 6: T_d monotonically decreases with increasing σ, and T_d is slightly smaller than T_c. The difference between

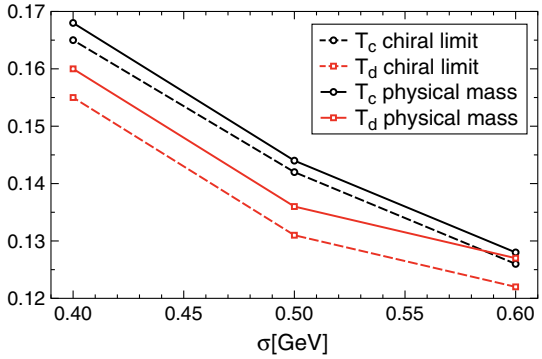

FIG. 6 (color online). The (pseudo)critical temperature T_c (black and marked by circles) and the deconfinement temperature T_d (red and marked by squares) vs the interaction width σ in the chiral limit (dashed lines) and for a physical current quark mass (full lines).

TABLE I. Critical temperatures of chiral symmetry restoration T_c and deconfinement T_d for different parameters (dimensionful quantities reported in GeV, $\Delta = T_c - T_d$).

σ	T_c^0	T_d^0	Δ^0/T_c^0	T_c^{m}	T_d^{m}	$\Delta^m/T_c^{\mathrm{m}}$
0.4	0.165	0.155	6.1%	0.168	0.160	4.8%
0.5	0.142	0.131	7.7%	0.144	0.136	5.6%
0.6	0.126	0.122	3.2%	0.128	0.127	0.8%
Average	0.144	0.136	5.7%	0.147	0.141	3.7%

T_d and T_c for a physical current quark mass is smaller than that obtained in the chiral limit. Specifically, when $\sigma \in [0.4, 0.6]$ GeV, we have $T_d \sim 94\% T_c$ in the chiral limit and $T_d \sim 96\% T_c$ with a physical light quark mass. The numerical results are presented in Table I. Our results are consistent with Ref. [18] which also found positivity violations of the Schwinger function below T_c.

By defining a confinement scale $r_\sigma = 1/\sigma$, it is apparent that both T_c and T_d increase with increasing r_σ, or $T_{c,d} \propto r_\sigma$. Considering that the difference between T_c and T_d is just several MeV, while the systematic uncertainty introduced by our approximations is certainly larger, it is reasonable to claim that chiral symmetry restoration and deconfinement coincide at nonzero temperature and zero chemical potential.

VI. SUMMARY AND REMARKS

At nonzero temperature and zero chemical potential, we computed the quark spectral function via the MEM from a solution of the QCD gap equation. For the latter, we used a rainbow interaction kernel which phenomenologically models recent results from DSE and lattice QCD. As a criterion for the positivity violation and restoration of the quark spectral function, we proposed an order parameter L_ρ which is directly related to the integral of the spectral function's negative part and obviously vanishes for positive definite spectral functions. We indeed found that $L_\rho > 0$ at low temperature while $L_\rho \equiv 0$ at high temperature; i.e., there exists a critical temperature T_d where L_ρ drops to zero. Here, the positivity of the quark spectral function is restored and quarks become asymptotic particles for $T > T_d$. Therefore, we conjecture that the deconfinement phase transition happens at $T = T_d$. Using our model setup, which can uniformly well describe vacuum properties of pseudoscalar and vector mesons with masses $\lesssim 1$ GeV, the critical temperature of deconfinement comes out slightly smaller than that of chiral symmetry restoration, i.e., $T_d \lesssim T_c$. Within the systematic uncertainties of our approach, however, it is reasonable to conclude that chiral symmetry restoration and deconfinement coincide.

It is generally expected that nuclear matter has a rich phase structure because of the interplay between DCSB and confinement at nonzero chemical potential. It would therefore be interesting to extend the present study to the case of nonzero chemical potential. The difference between T_c and T_d could then be more pronounced and give rise to the so-called quarkyonic phase [36,37].

ACKNOWLEDGMENTS

S.-x. Q. would like to thank C. S. Fischer and Y.-x. Liu for helpful discussions. The work of S.-x. Q. was supported by the Alexander von Humboldt Foundation through a Postdoctoral Research Fellowship.

[1] K. G. Wilson, Phys. Rev. D **10**, 2445 (1974).
[2] E. Eichten, K. Gottfried, T. Kinoshita, K. Lane, and T. Yan, Phys. Rev. D **17**, 3090 (1978).
[3] G. Bali, Phys. Rep. **343**, 1 (2001).
[4] G. Bali, H. Neff, T. Düssel, T. Lippert, and K. Schilling, Phys. Rev. D **71**, 114513 (2005).
[5] B. Svetitsky and L. G. Yaffe, Nucl. Phys. **B210**, 423 (1982).
[6] R. D. Pisarski, Phys. Rev. D **62**, 111501 (2000).
[7] E. Bilgici, F. Bruckmann, C. Gattringer, and C. Hagen, Phys. Rev. D **77**, 094007 (2008).
[8] C. S. Fischer, Phys. Rev. Lett. **103**, 052003 (2009).
[9] C. S. Fischer and J. A. Mueller, Phys. Rev. D **80**, 074029 (2009).
[10] C. D. Roberts, A. G. Williams, and G. Krein, Int. J. Mod. Phys. A **07**, 5607 (1992).
[11] C. D. Roberts and A. G. Williams, Prog. Part. Nucl. Phys. **33**, 477 (1994).
[12] C. D. Roberts, Prog. Part. Nucl. Phys. **61**, 50 (2008).
[13] P. Maris, Phys. Rev. D **52**, 6087 (1995).
[14] M. Bhagwat, M. Pichowsky, and P. C. Tandy, Phys. Rev. D **67**, 054019 (2003).
[15] W. Yuan, S.-x. Qin, H. Chen, and Y.-x. Liu, Phys. Rev. D **81**, 114022 (2010).
[16] R. K. Bryan, Eur. Biophys. J. **18**, 165 (1990).
[17] D. Nickel, Ann. Phys. (Amsterdam) **322**, 1949 (2007).
[18] J. A. Mueller, C. S. Fischer, and D. Nickel, Eur. Phys. J. C **70**, 1037 (2010).
[19] M. Asakawa, T. Hatsuda, and Y. Nakahara, Prog. Part. Nucl. Phys. **46**, 459 (2001).
[20] S.-x. Qin, L. Chang, Y.-x. Liu, C. Roberts, and D. Wilson, Phys. Rev. C **84**, 042202 (2011).
[21] S.-x. Qin, L. Chang, Y.-x. Liu, C. D. Roberts, and D. J. Wilson, Phys. Rev. C **85**, 035202 (2012).
[22] A. Aguilar, D. Binosi, J. Papavassiliou, and J. Rodríguez-Quintero, Phys. Rev. D **80**, 085018 (2009).
[23] A. Aguilar, D. Binosi, and J. Papavassiliou, Phys. Rev. D **86**, 014032 (2012).

[24] P. O. Bowman, U. M. Heller, D. B. Leinweber, M. B. Parappilly, and A. G. Williams, Phys. Rev. D **70**, 034509 (2004).
[25] O. Oliveira and P. Bicudo, J. Phys. G **38**, 045003 (2011).
[26] Ph. Boucaud, M. E. Gómez, J. P. Leroy, A. Le Yaouanc, J. Micheli, O. Pène, and J. Rodríguez-Quintero, Phys. Rev. D **82**, 054007 (2010).
[27] S.-x. Qin, L. Chang, Y.-x. Liu, and C. Roberts, Phys. Rev. D **84**, 014017 (2011).
[28] A. Bender, C. D. Roberts, and L. v. Smekal, Phys. Lett. B **380**, 7 (1996).
[29] M. Hobson and A. Lasenby, Mon. Not. R. Astron. Soc. **298**, 905 (1998).
[30] A. Balandin and A. Kaneko, Inverse Probl. **15**, 445 (1999).
[31] S. F. Gull and J. Skilling, *Quantified Maximum Entropy MemSys5 Users Manual* (Maximum Entropy Data Consultants Ltd., Suffolk, 1999).
[32] S.-x. Qin, L. Chang, H. Chen, Y.-x. Liu, and C. D. Roberts, Phys. Rev. Lett. **106**, 172301 (2011).
[33] Y. Aoki, S. Borsányi, S. Dürr, Z. Fodor, S. D Katz, S. Krieg, and K. Szabo, J. High Energy Phys. 06 (2009) 088.
[34] M. Le Bellac, *Thermal Field Theory* (Cambridge University Press, Cambridge, England, 2000).
[35] H. Song and U. Heinz, J. Phys. G **36**, 064033 (2009).
[36] L. McLerran and R. D. Pisarski, Nucl. Phys. **A796**, 83 (2007).
[37] L. McLerran, K. Redlich, and C. Sasaki, Nucl. Phys. **A824**, 86 (2009).